STRUCTURE AND BREAKDOWN OF INVARIANT TORI IN A 4-D MAPPING MODEL OF ACCELERATOR DYNAMICS

M. N. VRAHATIS, H. ISLIKER and T. C. BOUNTIS

Center for Research and Applications of Nonlinear Systems,
Department of Mathematics, University of Patras,
GR–261.10 Patras, Greece

We study sequences of periodic orbits and the associated phase space dynamics in a 4-D symplectic map of interest to the problem of beam stability in circular particle accelerators. The increasing period of these orbits is taken from a sequence of rational approximants to an incommensurate pair of irrational rotation numbers of an invariant torus. We find stable (elliptic–elliptic) periodic orbits of very high period and show that smooth *rotational tori* exist in their neighborhood, on which the motion is regular and bounded at large distances away from the origin. Perturbing these tori in parameter and/or initial condition space, we find either chains of smaller rotational tori or certain twisted tube-like tori of remarkable morphology. These tube-tori and tori chains have small scale chaotic motions in their surrounding vicinity and are formed about *invariant curves* of the 4-D map, which are either single loops or are composed of several disconnected loops, respectively. These smaller chaotic regions as well as the non-smoothness properties of large rotational tori under small perturbations, leading to eventual escape of orbits to infinity, are studied here by the computation of correlation dimension and Lyapunov exponents.

1. Introduction

One of the most challenging problems facing nonlinear science today is the extension of our knowledge of low-dimensional dynamics to problems which involve several degrees of freedom. This is particularly true in the case of conservative (e.g. Hamiltonian) systems, in which new and more complicated phenomena are expected in higher dimensions.

As is well known, Hamiltonian systems of $n \geq 2$ degrees of freedom have been studied extensively in the context of celestial mechanics, especially with regard to problems of galactic dynamics [Hénon & Heiles, 1964; Contopoulos *et al.*, 1982; Contopoulos & Magnenat, 1985; MacKay & Meiss, 1986]. In such systems, one of the most fruitful approaches is to examine the intersections of orbits with a $2N(= 2n - 2)$-dimensional Poincaré "surface" of section, on which the flow is reduced to a $2N$-dimensional ($2N$-D) symplectic mapping [Lichtenberg & Lieberman, 1983].

Another very important application concerns the stability of particle beams in high energy hadron colliders, where symplectic mappings naturally arise due to the periodically repeated (and of very brief duration) effects of beam–beam collisions, or beam passage through magnetic focusing elements [Corrigan *et al.*, 1982; Turchetti & Scandale, 1991; Bountis & Tompaidis, 1991].

The main open problems in such mappings — particularly in the $N(\geq 2)$-dimensional case — concern the *long term stability* of orbits, which can slowly diffuse away from the origin through thin chaotic layers, leading e.g. to stars escaping from a galaxy or particle loss in the storage rings of an accelerator.

An important hindrance to this weak instability phenomenon is provided by the presence of

invariant tori, or smooth N-dimensional surfaces on which the motion remains bounded for all time. In between these tori, however, there are small scale chaotic regions through which orbits can eventually "leak" to large distances, while the tori furthest away from the origin lose their smoothness under small perturbations yielding orbits which rapidly escape to infinity.

It is the purpose of this paper to study the structure and breakdown properties of such invariant tori in the case of a symplectic mapping of direct relevance of the beam stability problem in circular accelerators like the LHC (Large Hadron Collider) machine at CERN. As far as the physics of this application is concerned, our main conclusion — in agreement with many other studies [Corrigan *et al.*, 1982; Turchetti & Scandale, 1991] — is that there are large regions (with respect to the beam's aperture) around the circular path of the beam, in which the motion is extremely stable, in the sense that no significant diffusion of orbits away from this path is observed.

More generally, in the case of symplectic maps, many fascinating results have been obtained regarding the bifurcation properties of periodic orbits and the structure of invariant curves especially in the case of 2-D area-preserving maps satisfying the so-called twist condition [MacKay & Meiss, 1986]. In view of their many possible applications, it is natural to ask how these dynamical phenomena are extended to the $2N (> 4)$-D higher-dimensional case [Turchetti & Scandale, 1991; Bountis & Tompaidis, 1991; Vrahatis *et al.*, 1996].

In this paper, we continue the work started in a recent publication [Vrahatis *et al.*, 1996] and address the question of the structure and breakdown of invariant tori of 4-D symplectic maps which need not satisfy globally the twist condition. In particular, we concentrate on the example

$$T: \begin{pmatrix} x'_1 \\ x'_2 \\ x'_3 \\ x'_4 \end{pmatrix} = \begin{pmatrix} \cos\omega_1 & -\sin\omega_1 & 0 & 0 \\ \sin\omega_1 & \cos\omega_1 & 0 & 0 \\ 0 & 0 & \cos\omega_2 & -\sin\omega_2 \\ 0 & 0 & \sin\omega_2 & \cos\omega_2 \end{pmatrix}$$

$$\times \begin{pmatrix} x_1 \\ x_2 + x_1^2 - x_3^2 \\ x_3 \\ x_4 - 2x_1 x_3 \end{pmatrix}, \qquad (1)$$

which describes the (instantaneous) effect experienced by a hadronic particle as it passes through a

magnetic focusing element of the FODO cell type [Turchetti & Scandale, 1991; Bountis & Tompaidis, 1991]. x_1 and x_3 are the particle's deflections from the ideal (circular) orbit, in the horizontal and vertical directions respectively, and x_2, x_4 are the associated "momenta", while ω_1, ω_2 are related to the accelerator's betatron frequencies (or "tunes") q_x, q_y by

$$\omega_1 = 2\pi q_x, \quad \omega_2 = 2\pi q_y, \qquad (2)$$

and constitute the main parameters that can be varied by an experimentalist.

As (1) is essentially equivalent to a periodically driven 2-degree of freedom (or the Poincaré map of a 3-degree of freedom) Hamiltonian system, its 4-D phase space motion is expected to occur typically on 2-D invariant surfaces, characterized by two incommensurate rotation numbers (σ_1, σ_2), which approach (q_x, q_y) as $x_i \to 0$, $i = 1, \ldots, 4$. If these surfaces surround the origin in the form of 2-D tori, in 3-D projections, we call them *rotational* [see Fig. 1(a)] and ask how far from $(0, 0, 0, 0)$ they can still be found to exist. This question is of great importance to applications since, even though these 2-D tori do not "foliate" the 4-D phase space, they "surround" a region of the origin, where the dynamics is remarkably *stable*, in the sense that orbits starting within this region are seen to remain bounded even after 10^8 iterations of (1)!

As one perturbs such rotational tori, however, either in parameter or initial condition space, the following can occur:

(i) Either a "chain" of rotational tori of smaller size appears, in the form of vertical slices and of the same shape as the large torus [see Fig. 1(b)],

(ii) or the orbit forms a twisted, tube-like torus, wrapped "horizontally" around the large torus [see Fig. 1(c)],

(iii) or, if the original torus is close to some chaotic (or escape) region, points begin to drift and scatter about in an irregular fashion showing visible nonsmoothness properties and torus breakdown [see Fig. 1(d)].

Cases (i) and (ii) above have also been observed by other researchers in 3-degree of freedom Hamiltonian systems [Contopoulos *et al.*, 1982; Contopoulos & Magnenat, 1985].

In Sec. 2, we begin with a brief outline of our approach to the study of invariant tori via the computation of sequences of periodic orbits as we have
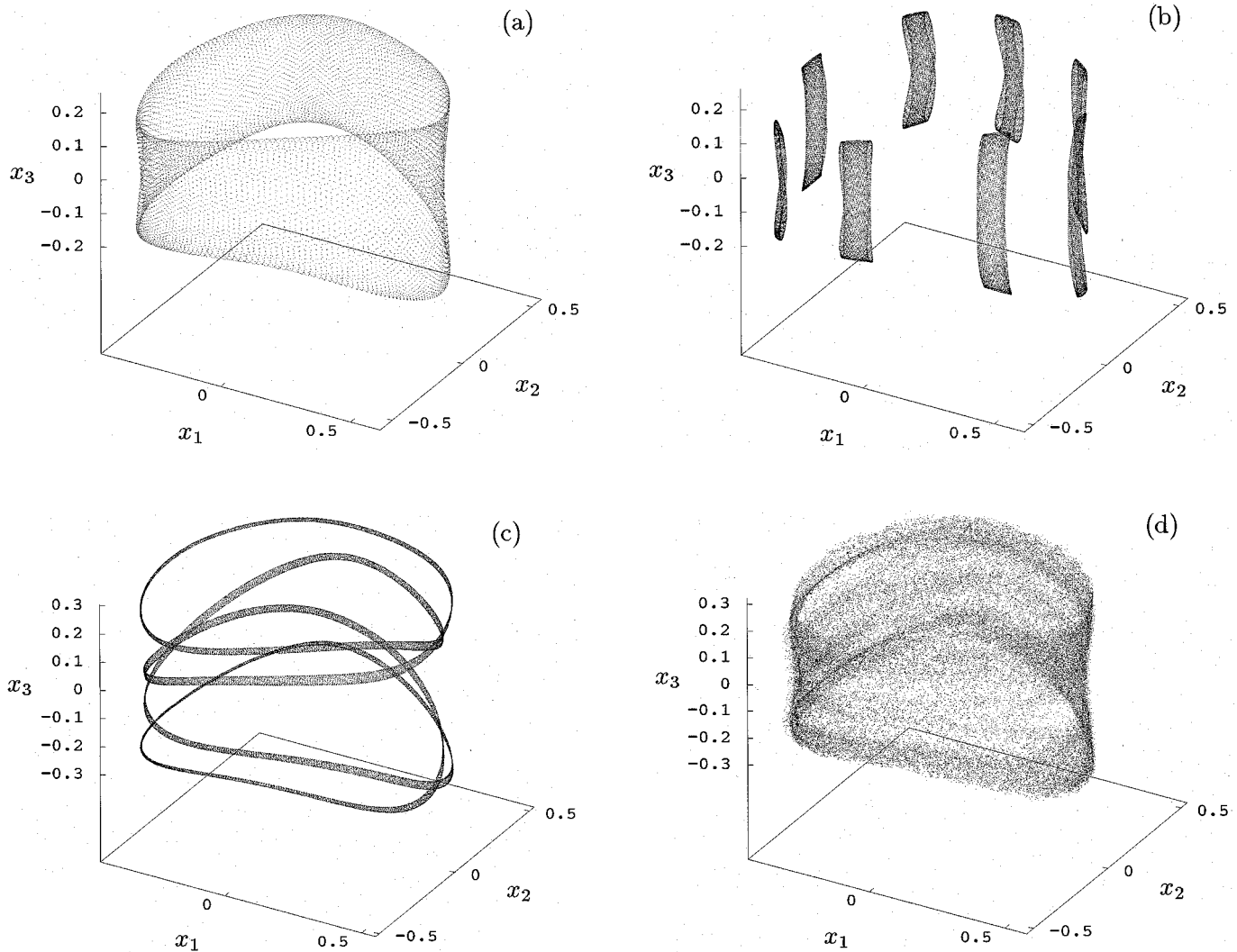
Fig. 1. Projection of different orbits into x_1–x_2–x_3 space, with 50 000 points plotted for (b)–(d): (a) Period 13 327 EE orbit; (b) initial conditions as in (a), with q_x disturbed by -0.001; (c) initial conditions of the period 16 127a orbit, with x_1 disturbed by 0.025; (d) orbit with the initial condition as in (c), but x_1 disturbed now by 0.005.

done in a recent publication [Vrahatis *et al.*, 1996]. We then describe our interesting observation that the tori of cases (i) and (ii) above are formed about invariant curves, which either are a number of disconnected loops in a direction "vertical" to the x_1, x_2 plane [in case (i)], or are connected in a single one-dimensional loop in 4-D space [in case (ii)]. We also discuss in that section the role of rotation numbers and the possible validity of a generalized Greene's criterion [Greene, 1979; MacKay, 1983] for higher-dimensional symplectic maps [Tompaidis, 1995].

Then, in Sec. 3, we present our results on the analysis of torus breakdown by showing how estimates of the correlation dimension, D_2, can reflect the chaotic properties of orbits in the vicinity of

large invariant tori, like the one shown in Fig. 1(d): A value of D_2 larger than 2, positive Lyapunov exponents, and non-stationary behavior of orbits are obtained successively after $k \times 10^4$, $k = 1, 2, \ldots$ iterations of the map. These results are warning signs that one is close to unbounded motion and escape away from the torus, as occurs indeed in many cases, after a sufficiently high number of iterations.

We also present, in Sec. 3, similar evidence of (small-scale) chaotic behavior in the vicinity of tube-tori and chains of tori and argue, using cross-sections of the 4-D space, that these two cases represent extensions of the island chains found near higher order resonances of 2-D area preserving maps. Finally, in Sec. 4, we summarize our findings and offer some concluding remarks.

2. Approximating Invariant Tori by Periodic Orbits

Consider an N-dimensional mapping of the form:

$$X' = T(X), \quad X = (x_1, x_2, \ldots, x_N), \quad (3)$$

like (1) for $N = 4$. If $N = 2k$ and X, X' are related by a generating function

$$F = F(x_1, x_3, \ldots, x_{2k-1}, x'_1, x'_3, \ldots, x'_{2k-1}), \quad (4)$$

according to the expressions [Kook & Meiss, 1989]

$$x'_{2i} = \frac{\partial F}{\partial x'_{2i-1}}, \quad x_{2i} = -\frac{\partial F}{\partial x_{2i-1}}, \quad i = 1, 2, \ldots, k, \quad (5)$$

then (3) is called *symplectic* and its dynamics corresponds to that of a $(k + 1/2)$-degree-of-freedom Hamiltonian system: Its quasiperiodic orbits lie on k-dimensional tori embedded in a $2k$-dimensional phase space and, for $k > 1$, chaotic orbits can, in principle, leak through these tori, hence global stability in their neighborhood cannot be guaranteed.

It is easy to show that our accelerator map (1) is symplectic with the generating function

$$F = -\frac{\cos \omega_1}{2 \sin \omega_1}(x'^2_1 + x^2_1) - \frac{\cos \omega_2}{2 \sin \omega_2}(x'^2_3 + x^2_3)$$

$$+ \frac{x_1 x'_1}{\sin \omega_1} + \frac{x_3 x'_3}{\sin \omega_2} + \frac{x^3_1}{3} - x_1 x^2_3. \quad (6)$$

Our aim here is to understand the structure of the 2-D tori of (1) in the (x_1, x_2, x_3, x_4) space and to study the properties of the motion in the neighborhood of these tori.

To do this, we shall construct sequences of periodic orbits of (1) whose period r_n is taken from a sequence of rational rotation numbers

$$(\sigma^{(n)}_1, \sigma^{(n)}_2) = \left(\frac{p_n}{r_n}, \frac{q_n}{r_n}\right), \quad n = 0, 1, 2, \ldots, \quad (7)$$

which converge, as $n \to \infty$, to a pair of incommensurate irrationals. In the problem studied here, we have chosen the example:

$$(\sigma^{(n)}_1, \sigma^{(n)}_2) \xrightarrow[n \to \infty]{} (\sigma_1, \sigma_2)$$

$$= \left(\frac{\sqrt{5} - 1}{2}, \sqrt{2} - 1\right)$$

$$= (0.61803\ldots, 0.41421\ldots). \quad (8)$$

The choice of σ_1, σ_2 in (8) is arbitrary. However, as it includes the "golden mean" σ_1, it may be useful

for comparison purposes with the 2-D case [Greene, 1979; MacKay, 1983; MacKay & Meiss, 1986; Tompaidis, 1995].

Selecting now linear frequencies q_x, q_y for our map, close to the values in (8),

$$q_x = 0.61903, \quad q_y = 0.4152, \quad (9)$$

we shall attempt to approximate the (σ_1, σ_2)-invariant torus by periodic orbits characterized by the rotation numbers of the Jacobi–Perron sequence [Bernstein, 1971; Schweiger, 1973]: These are recursively obtained from the relation:

$$s_{n+1} = k_{n+1} s_n + l_{n+1} s_{n-1} + s_{n-2}, \quad n = 0, 1, \ldots, \quad (10)$$

$(s_n = p_n, q_n, r_n)$, with the integers k_n, l_n determined by the map:

$$(s^{(n+1)}_1, s^{(n+1)}_2) = \left(\left\{\frac{1}{s^{(n)}_2}\right\}, \left\{\frac{s^{(n)}_1}{s^{(n)}_2}\right\}\right),$$

$$(k_{n+1}, l_{n+1}) = \left(\left[\frac{1}{s^{(n)}_2}\right], \left[\frac{s^{(n)}_1}{s^{(n)}_2}\right]\right), \quad (11)$$

where $[x]$ and $\{x\}$ refer to the integer and fractional part of x respectively, and

$$(s^0_1, s^0_2) = (\sigma_1, \sigma_2),$$

$$(p_0, q_0, r_0) = (0, 0, 1),$$

$$(p_{-1}, q_{-1}, r_{-1}) = (1, 0, 0), \quad (12)$$

$$(p_{-2}, q_{-2}, r_{-2}) = (0, 1, 0).$$

In Table 1 we exhibit Jacobi–Perron approximants to the irrationals (8), up to $n = 16$, cf. (7). Note that the convergence is rather slow, as one might expect of quadratic irrationals, like σ_1, σ_2.

In order to compute these r_n-periodic orbits, we make use of a recently developed method, which has already been successfully applied to locate long periodic orbits of this map [Vrahatis *et al.*, 1996]. This method exploits topological degree theory to provide a criterion for the existence of a periodic orbit of an iterate of the map within a given region (the CP (characteristic polyhedron)-criterion). It is especially useful for the computation of high period orbits and quite efficient, since the only computable information required is the algebraic sign of the components of the mapping. Thus, it is not significantly affected by the unavoidable inaccuracies of the calculations in the neighborhood of unstable

Table 1. Rational approximants of the Jacobi–Perron algorithm of the quadratic irrationals $\sigma_1 = (5^{1/2} - 1)/2 = 0.61803\ldots$ and $\sigma_2 = 2^{1/2} - 1 = 0.41421\ldots$ and the period p of the corresponding periodic orbit.

n	p_n	q_n	$p_n/r_n - \sigma_1$	$q_n/r_n - \sigma_2$	$p = r_n$
4	1	1	-0.11803399	$0.85786438 \times 10^{-1}$	2
5	3	2	0.13196601	$0.85786438 \times 10^{-1}$	4
6	3	2	$-0.18033989 \times 10^{-1}$	$-0.14213562 \times 10^{-1}$	5
7	91	61	$-0.31691239 \times 10^{-2}$	$-0.20514002 \times 10^{-2}$	148
8	94	63	$0.38706388 \times 10^{-3}$	$0.26012184 \times 10^{-3}$	152
9	755	506	$0.31162960 \times 10^{-3}$	$0.20085204 \times 10^{-3}$	1221
10	846	567	$-0.64668078 \times 10^{-4}$	$-0.42634689 \times 10^{-4}$	1369
11	940	630	$-0.19524582 \times 10^{-4}$	$-0.12378941 \times 10^{-4}$	1521
12	8181	5483	$0.63527172 \times 10^{-5}$	$0.41606759 \times 10^{-5}$	13 237
13	9027	6050	$-0.30396282 \times 10^{-6}$	$-0.22538829 \times 10^{-6}$	14 606
14	9967	6680	$-0.21167340 \times 10^{-5}$	$-0.13716371 \times 10^{-5}$	16 127
15	37 142	24 893	$0.18932888 \times 10^{-6}$	$0.12549818 \times 10^{-6}$	60 097
16	83 311	55 836	$0.13587919 \times 10^{-6}$	$0.87478537 \times 10^{-7}$	134 800

periodic orbits and can be briefly described as follows: Suppose we want to find periodic orbits of a nonlinear mapping $T : \mathcal{D} \subset \mathbb{R}^N \to \mathbb{R}^N$ of period p, i.e. fixed points $X^\star = (x_1^\star, x_2^\star, \ldots, x_N^\star) \in \mathcal{D}$ of T^p, satisfying the following system of equations:

$$\Phi_N(X^\star) = \mathcal{O}_N = (0, 0, \ldots, 0)\,, \qquad (13)$$

with $\Phi_N = (f_1, f_2, \ldots, f_N) = T^p - I_N$, where I_N is the N-D identity mapping. An N-complete matrix $\mathcal{M}_N$ is defined as a $2^N \times N$ matrix whose rows are formed by all possible combinations of $-1, 1$. The N-polyhedron $\Pi^N = \langle \Upsilon_1, \Upsilon_2, \ldots, \Upsilon_{2^N} \rangle$ with vertices Υ_i in $\mathbb{R}^N$ is called a *characteristic polyhedron* (*CP*) *relative to* Φ_N if the matrix of signs associated with Φ_N and Π^N, $\mathcal{S}(\Phi_N; \Pi^N)$, is identical with the N-complete matrix $\mathcal{M}_N$ [Vrahatis, 1988]. In other words, at the 2^N vertices of Π^N the signs of $\Phi_N(\Upsilon_i)$, $i = 1, 2, \ldots, 2^N$ yield every combination of ± 1.

If Π^N is a CP then, under suitable assumptions on the boundary of Π^N, the value of the topological degree of Φ_N at $\mathcal{O}_N$ relative to Π^N is nonzero, which implies the existence of a periodic orbit inside Π^N. For a detailed description of how to construct a CP and locate a desired periodic orbit see [Vrahatis, 1988; Vrahatis *et al.*, 1993; Vrahatis & Bountis, 1994; Vrahatis, 1995; Drossos *et al.*, 1996].

A generalized bisection method can then be employed in combination with the CP-criterion, to bisect a CP, in such a way that the new refined N-polyhedron is also a CP. To do this, one computes

the midpoint of an edge of Π^N and uses it to replace that vertex of Π^N, for which the signs with respect to Φ_N are identical with the ones of the midpoint. Finally, the number ν of bisections of the edges of a Π^N required to obtain a new refined CP, $\Pi_\star^N$, whose longest edge length, $\Delta(\Pi_\star^N)$, satisfies $\Delta(\Pi_\star^N) \leq \varepsilon$, for some $\varepsilon \in (0, 1)$, can be shown to be given by $\nu = [\log_2(\Delta(\Pi^N)\varepsilon^{-1})] + 1$ (see [Vrahatis, 1988]).

Applying the CP-criterion to our map (1), we construct a sequence of periodic orbits of period $p = r_n$, taken from the last column of Table 1, and determine their stability by computing the eigenvalues λ_i of the determinant of the return Jacobian matrix from the equation

$$\det(DT^p - \lambda E_4) = 0\,, \qquad (14)$$

where E_4 is the 4×4 identity matrix. We distinguish five cases depending on the values of the λ_i's [Todesco, 1994; Vrahatis *et al.*, 1996]:

(i) All $\lambda_i \in \mathbb{C}$, $|\lambda_i| = 1$: Elliptic–Elliptic (EE);
(ii) two λ_i's $\in \mathbb{C}$ with $|\lambda_i| = 1$, and two λ_i's $\in \mathbb{R}$:

  (a) Elliptic–Hyperbolic (EH) if the magnitude of the projection of the *real* eigenvectors is largest in the x_3, x_4 plane;
  (b) Hyperbolic–Elliptic (HE) if the magnitude of the projection of the *real* eigenvectors is largest in the x_1, x_2 plane;

(iii) all $\lambda_i \in \mathbb{R}$, $|\lambda_{1,3}| < 1$, $|\lambda_{2,4}| > 1$: Hyperbolic–Hyperbolic (HH);

(iv) all $\lambda_i \in \mathbb{C}$, $|\lambda_{1,2}| < 1$, $|\lambda_{3,4}| > 1$: Complex Unstable (CU).

Since we are interested in approximating a smooth torus, according to Greene's criterion for 2-D maps [Greene, 1979; MacKay & Meiss, 1986], we need to be concerned only with EE orbits, category (i). Indeed, using our methods, we were able to compute a sequence of r_n-periodic EE orbits, (with periods as in Table 1), whose eigenvalues, for $n \geq 11$, were found to be very close to $\mathrm{Re}(\lambda_i) = 1$.

First of all, let us start by clarifying that although the period r_n of our orbits is taken from the Jacobi–Perron sequence, (10)–(12), there is no reason why the rotation numbers of our orbits should have the same p_n, q_n as dictated by this sequence. Indeed, by independent calculations, using Laskar's method of frequency analysis [Laskar *et al.*, 1992; Laskar, 1993; Papaphilippou, 1996] it can be verified that the *actual* rotation numbers of our orbits are *not* the corresponding ones of Table 1 (see Table 2). Furthermore, it does not appear easy to compute periodic orbits of our 4-D map for any *given* rotation number pair, by the CP, or any other method.

Thus, it is not possible to follow a specific sequence of converging periodic orbits (like the Jacobi–Perron of Table 1) and locate the (σ_1, σ_2) torus we originally set out to find. Still, the high period orbits we do find have rotation numbers close to (σ_1, σ_2) and eigenvalues whose real part approaches 1, as the period increases. This suggests that there are invariant tori in their neighborhood, which are smooth and can guarantee the stability of orbits lying on them, for all time. The initial conditions and eigenvalues of the return Jacobian for a number of EE periodic orbits of increasing period are listed here in Table 3.

Let us now examine more closely some of these EE orbits: As we see in Fig. 2, there are examples of rotational type [periods 1521, 13 237, 16 127a,b in Fig. 2(a)] and of the tube and invariant curve type [periods 14 606 and 1221 in Figs. 2(a) and 2(b) respectively]. In Figs. 3(a) and 3(b) we plot their points (and the points of some more orbits) lying in a "cross-section" about the x_1, x_2 plane, for $|x_3| \leq 0.04$ and x_4 arbitrary.

Observe, in Fig. 3, that there are some evident similarities with the case of 2-D maps: Rotational tori play a role similar to that of invariant curves surrounding the origin in the 2-D case, while tube-tori, like those of Fig. 1(c) and Fig. 2(a), correspond to island chains [see Fig. 3(a)]. In 4-D, however, one also finds (upon perturbation of large tori) chains of smaller rotational tori, as shown e.g. in Fig. 1(b). Such chains of tori are commonly observed upon perturbation of a large rotational torus. Moreover, as we describe in the next section, it is possible to observe small scale chaotic behavior in the vicinity of these tube-tori and tori chains, similar to the thin chaotic regions surrounding the island chains of area-preserving maps [see Fig. 3(b)].

Finally, what about these periodic orbits like the one of period 1221, whose points lie on a curve in 4-D space? What is the dynamics in the neighborhood of that curve? To answer this question we perturb slightly the initial conditions of the 1221 orbit of Fig. 2(b) and obtain a tube-torus about it, similar to the one shown in Fig. 4(a).

Conversely, we can start with a tube-orbit like the one shown in Fig. 2(a) and ask what is the

Table 2.   Rotation numbers of the considered periodic orbits.

	From Table 1		From Frequency Analysis	
Period	p_n/r_n	q_n/r_n	Rot. Num. 1	Rot. Num. 2
148	0.6148648	0.4121621	0.6081081	0.4121621
152	0.6184210	0.4144736	0.5986842	0.4210526
1221	0.6183456	0.4144144	0.8615888	0.4307944
1369	0.6179693	0.4141709	0.5902118	0.4243973
1521	0.6180144	0.4142011	0.6002629	0.4247205
13 237	0.6180403	0.4142177	0.6262748	0.4031880
14 606	0.6180336	0.4142133	0.6107763	0.4160618
16 127a	0.6180318	0.4142121	0.6228064	0.4065852
16 127b	0.6180318	0.4142121	0.6078625	0.4215291

Table 3. Initial conditions X_0 of EE periodic orbits and their corresponding eigenvalues λ_i, $i = 1, \ldots, 4$ of the return Jacobian.

p	X_0	$\text{Re}(\lambda_i)$	$\text{Im}(\lambda_i)$
148	−0.350618075038668	0.747592162322379	−0.664158082713847
	−0.044755653513320	0.747592162322379	0.664158082713847
	−0.293566057531218	0.946563288783641	−0.322518124028874
	0.630466527671912	0.946563288783641	0.322518124028874
152	−0.130463565655997	0.336026480609178	−0.941852538526940
	0.299819322230460	0.336026480609178	0.941852538526940
	0.349001756567030	0.993961422946604	−0.109730076524334
	0.581486596549853	0.993961422946604	0.109730076524334
1221	−0.205038258262312	0.999999999998525	−0.000001809133065
	0.255949570906002	0.999999999998525	0.000001809133065
	−0.653912472912163	−0.891356893634381	−0.453302204021261
	0.436600752242947	−0.891356893634381	0.453302204021261
1369	−0.332673393161558	−0.465407497378064	−0.885096526588194
	0.102350030928628	−0.465407497378064	0.885096526588194
	−0.500963713749919	−0.600414236221095	−0.799689155213452
	0.650306028375437	−0.600414236221095	0.799689155213452
1521	−0.182766867426596	0.990541256588061	−0.137215229757129
	0.066896173589127	0.990541256588061	0.137215229757129
	−0.590556627456845	0.999999987202442	−0.000159108927349
	0.032513902428680	0.999999987202442	0.000159108927349
13 237	0.613394867338782	0.999999997219058	−0.000073999461113
	−0.144995505996665	0.999999997219058	0.000073999461113
	−0.260453091758909	0.999999999871764	−0.000016001571496
	−0.162371436378303	0.999999999871764	0.000016001571496
14 606	0.281764312323398	0.999999999795389	−0.000020477598185
	0.092251013539143	0.999999999795389	0.000020477598185
	0.526461773405660	0.999999999974517	−0.000007145840906
	0.152466695071175	0.999999999974517	0.000007145840906
16 127a	0.180461376558454	0.999999459769476	−0.000941177914352
	0.354314078603677	0.999999459769476	0.000941177914352
	−0.154528284709671	0.999999882925977	−0.000528227739496
	−0.282077719425159	0.999999882925977	0.000528227739496
16 127b	0.046541280000730	0.999999999898236	−0.000012481547203
	0.041535332083140	0.999999999898236	0.000012481547203
	−0.028757985532270	0.999999999784125	−0.000023965312399
	−0.466442803661036	0.999999999784125	0.000023965312399
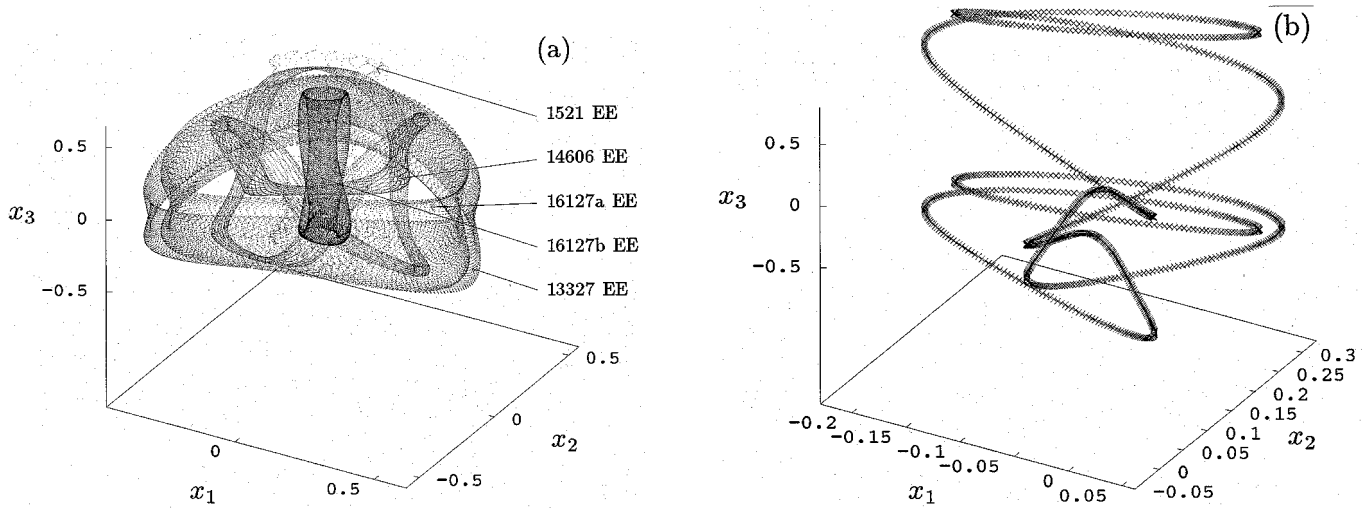
Fig. 2.   Projection of different periodic EE orbits into x_1–x_2–x_3 space: (a) Period 1521, period 13 327, period 14 606, period 16 127a, and the period 16 127b orbit; and (b) the period 1221 orbit, whose points are lying on a curve.
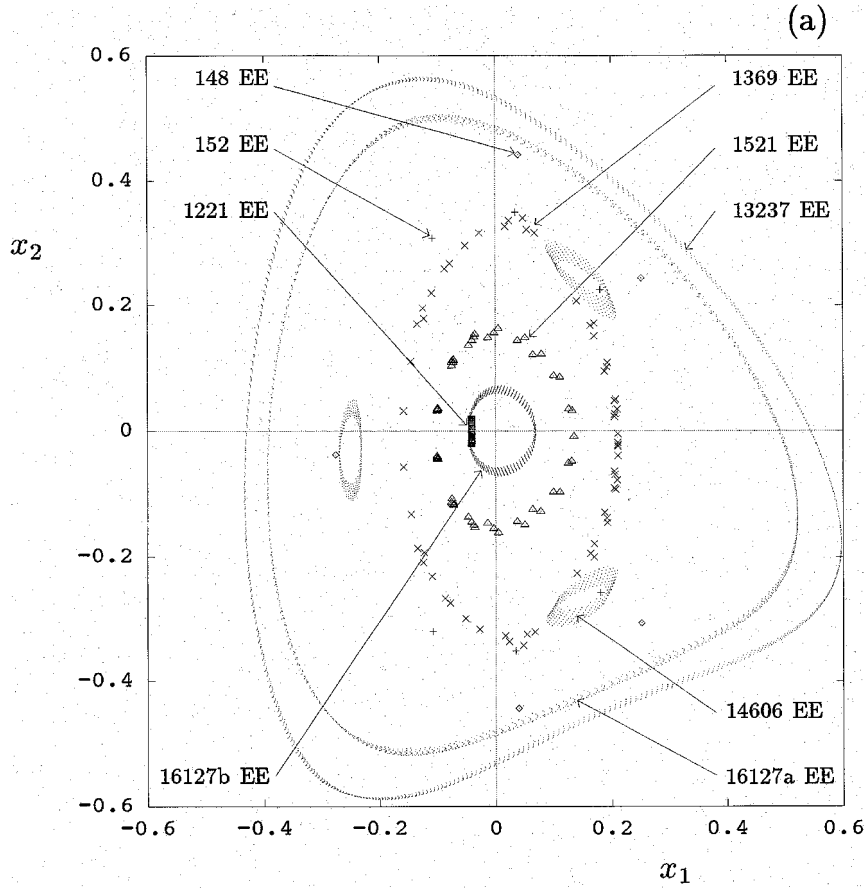
Fig. 3.   (a) Different periodic EE orbits whose "cross-section" is plotted in the x_1–x_2 plane, with $|x_3| \leq 0.04$ (x_4 arbitrary); (b) same "cross-section" as in (a) for the two perturbations of the period 13237 orbit shown in Fig. 1(b) and described in Fig. 8.
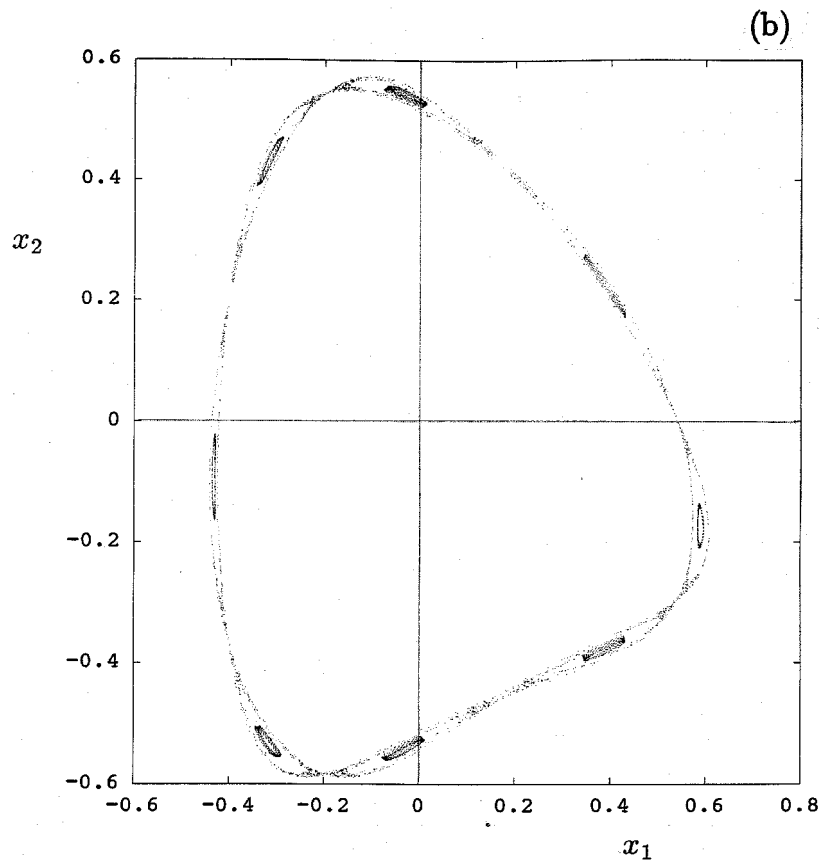
Fig. 3.   (*Continued*)
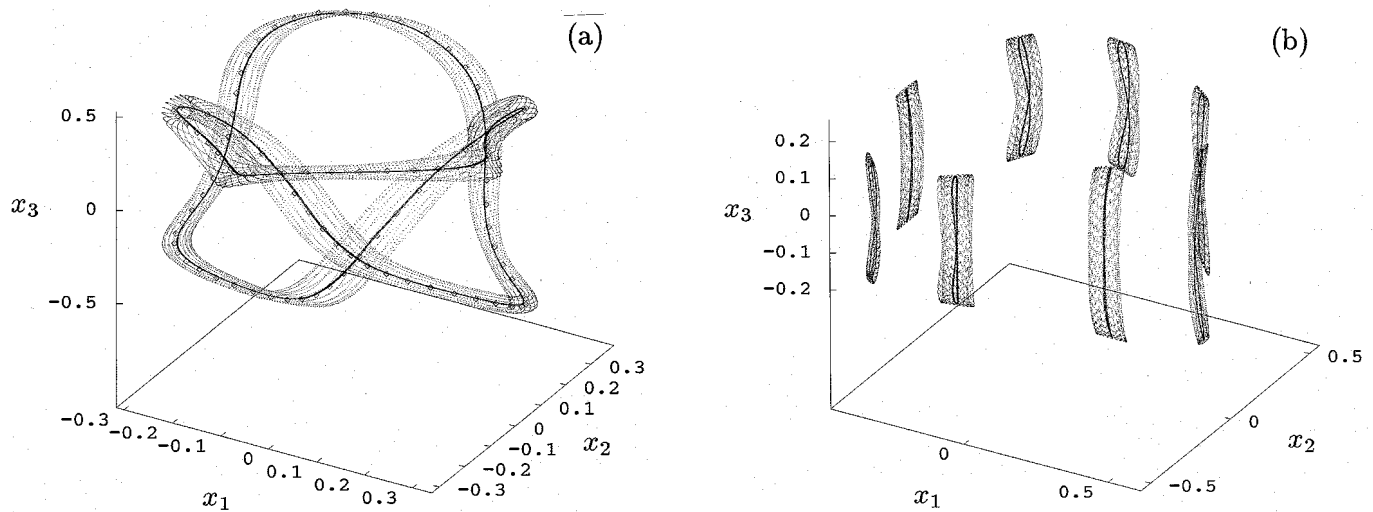
Fig. 4.   Projection into x_1–x_2–x_3 space: (a) The period 14 606 EE orbit, together with three orbits starting near the center of the tube. Two of these orbits form a single-loop invariant curve, each, while the third one (marked with ◇) is periodic with period 113; (b) a perturbation [$\Delta q_x = -0.001$; see Fig. 1(b)] of the period 13 237 orbit yielding a chain of eight small tori, in the "interior" of which one finds a set of disconnected multi-loop curves.

dynamics in its "interior": What we find are invariant thinner tubes, whose motion becomes more and more aligned with the axis of the tube, until they become invariant curves, or periodic orbits as shown in Fig. 4(a). The main feature of these invariant curves is that they form a *single loop* in 4-D space, albeit twisted around in a complicated way.

Finally, the corresponding dynamics of the chains of smaller rotational tori is similar. As we vary the initial conditions, proceeding towards their "interior", we find that they are also formed about a set of disconnected loops (or invariant curves), whose main direction is *vertical* to the x_1, x_2 plane, see Fig. 4(b).

3. Chaotic Behavior and Breakdown of Invariant Tori

Clearly the 4-D map studied in this paper, at the parameter values q_x, q_y we have chosen, has large regions of stable bounded motion around the origin. Chaotic behavior is expected to be confined within very small scale regions near unstable periodic orbits. Of course, the domain where it is likely to be most evident is far away from the origin, where the nonlinear terms are more significant and rapid escape of orbits to infinity becomes possible.

But where are these "limits" of bounded motion and how is escape of orbits related to the breakdown of invariant tori near these limits? Furthermore, how can we determine where the small scale chaotic regions lie and what tools can we use to study their properties?

To answer these questions, we shall first investigate the dynamics in the neighborhood of one of our EE periodic orbits, whose points are furthest away from the origin. Let us concentrate, in particular, on the period 13 237 orbit shown in Fig. 1(a) and consider different perturbations of its points under small variations of the initial conditions and parameters of the system. Here, we describe what happens under variations of the q_x parameter only, as all other types of perturbations yield similar results.

Fixing the initial conditions on those of the period 13 237 orbit at the q_x, q_y values cf. (9), we change only the horizontal tune by a small amount:

$$q'_x = q_x + \Delta q_x = 0.61903 + \Delta q_x . \qquad (15)$$

For $\Delta q_x \lesssim 0.005$ we obtain a quasiperiodic orbit in the form of a smooth rotational torus which
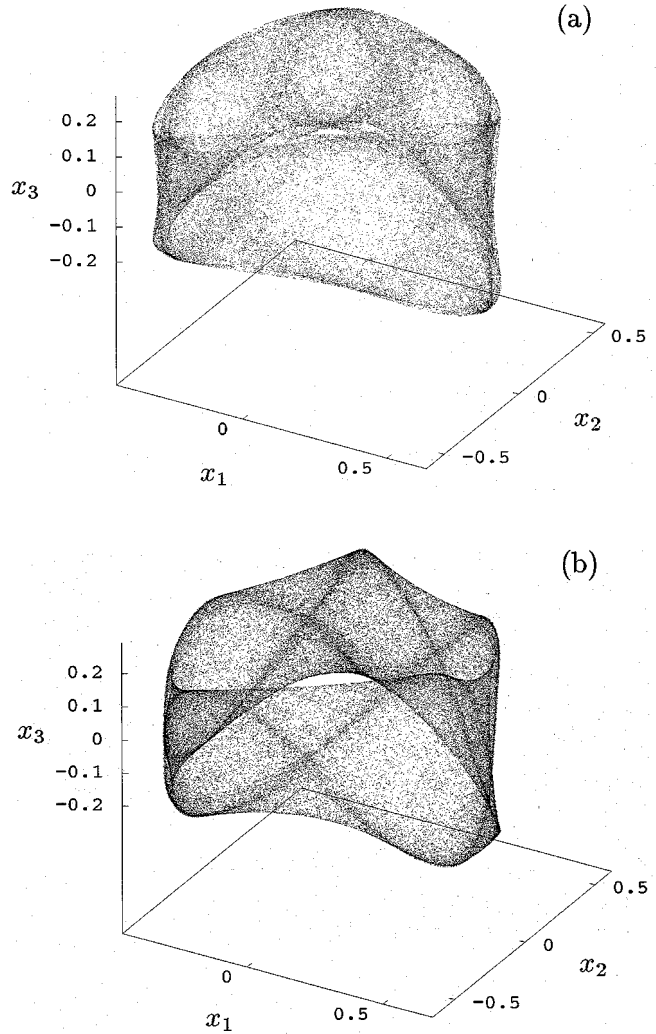
Fig. 5.   (a) Projection into x_1–x_2–x_3 space of the period 13 237 EE orbit of Fig. 1(a) with the frequency q_x perturbed by $\Delta q_x = 0.007$ (see (18); 50 000 points are plotted); (b) the same initial conditions as in (a), but with $\Delta q_x = 0.009585$ (80 000 points are plotted). This orbit diverges after 82 197 iterations (this value depends on the machine).

strongly resembles the $\Delta q_x = 0$ case, Fig. 1(a). However, already at $\Delta q_x \gtrsim 0.007$, we observe in Fig. 5(a) clear evidence of "irregular" behavior, as if the motion no longer lies on a smooth 2-D torus but tends to fill out a domain of dimension larger than 2. In fact, if we increase q'_x further — with $\Delta q_x = 0.009585$ in (15) — not only do we find similar nonsmoothness features, but the orbit also escapes to infinity after nearly 8×10^4 iterations! [see Fig. 5(b)].

To study the dynamics of these orbits more closely, we decided to calculate the correlation dimension [Grassberger & Procaccia, 1983a, 1983b] of a time series obtained by keeping the successive

iterates of an initial vector $X^{(0)}$,

$$S = \{X^{(0)}, X^{(1)}, X^{(2)}, \ldots, X^{(M)}\}, \quad M \gg 10^3,$$
(16)

under the mapping (1):

$$X^{(n+1)} = T(X^{(n)}),$$

$$X^{(n)} = (x_1^{(n)}, x_2^{(n)}, x_3^{(n)}, x_4^{(n)}), \quad n = 0, 1, \ldots, M,$$
(17)

cf. (3). Since the correlation dimension D_2 is a close estimate of the Hausdorff (fractal) dimension D_0 of the "surface" on which the orbit lies, we should expect $D_2 \simeq 2$ for a 2-D torus and $D_2 > 2$ for an

orbit that occupies a higher-dimensional region of the 4-D phase space.

Furthermore, if our series S, in (16), is part of a stationary process, its topological properties should not change as M increases beyond a number, say $M_0 = 5000$ for our 4-D map, which is needed for its topological invariants (dimensions, Lyapunov exponents, etc.) to converge to their corresponding values. However, if the motion starts to diffuse slowly away from 2-D, one would expect these quantities to change as M increases beyond M_0.

This is indeed what we observe in Figs. 5 and 6. As we describe in detail in the Appendix, the D_2 value corresponding to the orbit of Fig. 1(a) with a perturbation of $\Delta q_x = 0.001$ is estimated
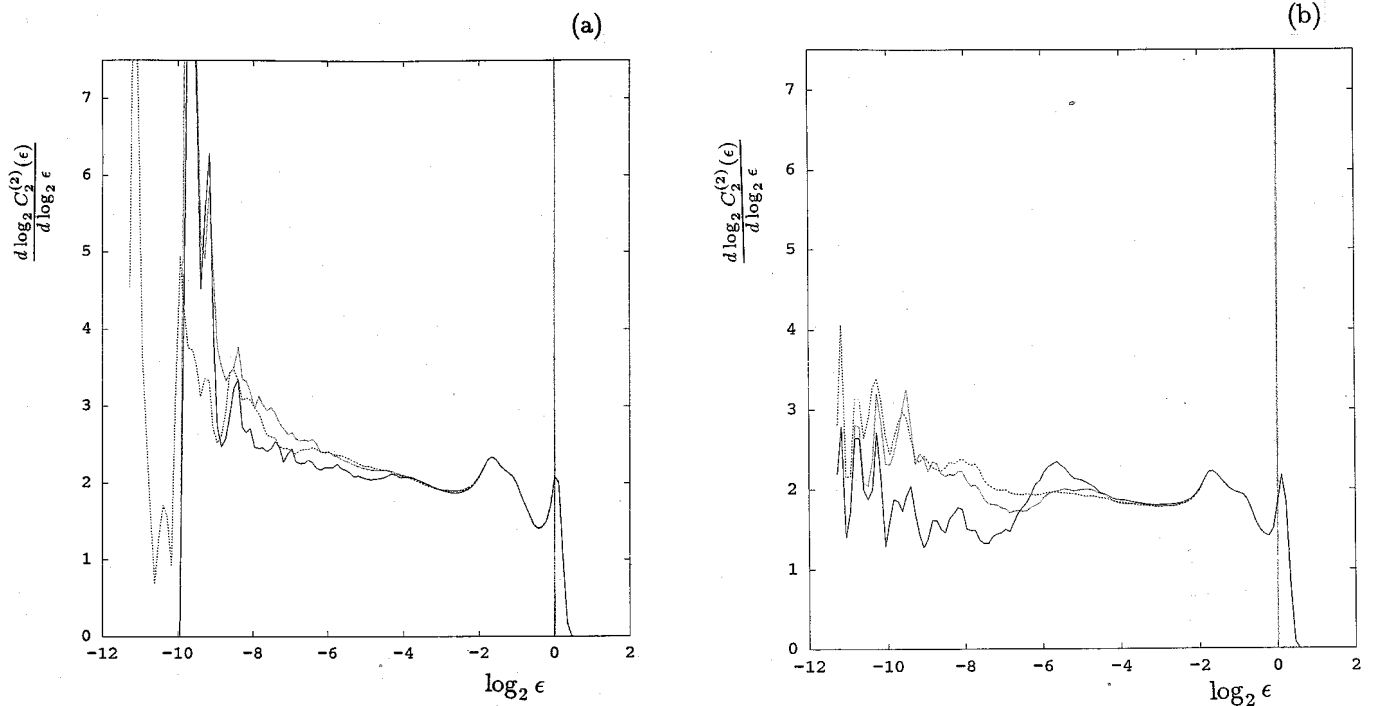
Fig. 6.   Correlation dimension estimates: Slope plots [see Appendix, (A3)] are shown, calculated by using the first 10 000 (solid), 20 000 (dashed), and 30 000 (short dashes) points in each of the following cases: (a) with $\Delta q_x = 0.007$ [see Fig. 5(a)]; (b) with $\Delta q_x = 0.009585$ [see Fig. 5(b)].

Table 4.   Correlation dimension of perturbations of periodic orbits.

Period	Correl. dim. D_2	Picture
1221	0.96 ± 0.09	invariant curve
1521	2.11 ± 0.18	rotational torus
13 237 (pert. in. cond.)	2.07 ± 0.05	rotational torus
14 606	2.36 ± 0.06	tube-torus
16 127a	2.06 ± 0.05	rotational torus
16 127b	2.12 ± 0.06	rotational torus
13 237 (pert. q_x)	2.11 ± 0.06	chain of 8 tori
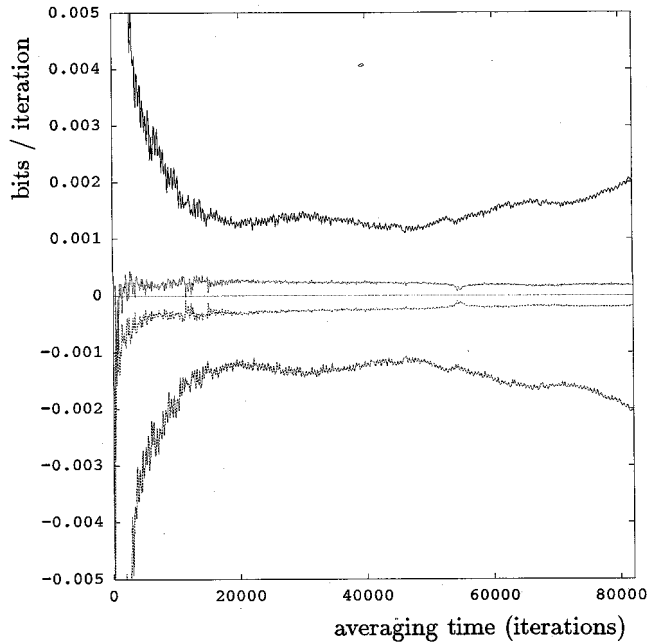
Fig. 7. Estimates of the four Lyapunov exponents Λ_i, using the algorithm described in the Appendix (cf. (A6), evolution time-step is 1, plotted is every 100th average). The initial conditions of the period 13 237 EE orbit are used with q_x perturbed by $\Delta q_x = 0.009585$ [see Figs. 5(b) and 6(b)]. Note how the slow outward diffusion of the orbits yield a maximum Lyapunov exponent which tends to grow on the average after 50 000 iterations.

by the large "plateau" in the plots of (A3) to be nearly 2 and remains approximately the same for $M = M_k = k \times 10^4$, $k = 1, 2, 3$ iterations of the map (see also Table 4). However, for $\Delta q_x = 0.007$, 0.009585 in Figs. 6(a) and 6(b), respectively, the "plateaus" occur at $D_2 > 2$ and exhibit nonstationary features: They are associated with plots, shown in Figs. 5(a) and 5(b) respectively, which differ as M increases from M_1 to M_2 and M_3 and clearly show a higher than 2-D structure.

Moreover, the Lyapunov exponents Λ_i, $i = 1, 2, 3, 4$ (see Appendix) which all go to zero on a 2-D invariant torus behave differently in the case of a nonsmooth, "irregular" orbit, as seen in Fig. 7: In particular the largest one of them is clearly positive and grows in value, as M increases, reflecting perhaps the diffusive character of the motion in a region of increasing dimension.

Let us now examine the dynamics in the vicinity of tube-tori and chains of rotational tori: First of all, concerning tube-like orbits like the one shown in Figs. 2(a) and 4(a) with period 14 606, we have observed that in their close neighborhood the value of the correlation dimension is found to be significantly higher than 2 (see Table 4). Furthermore,
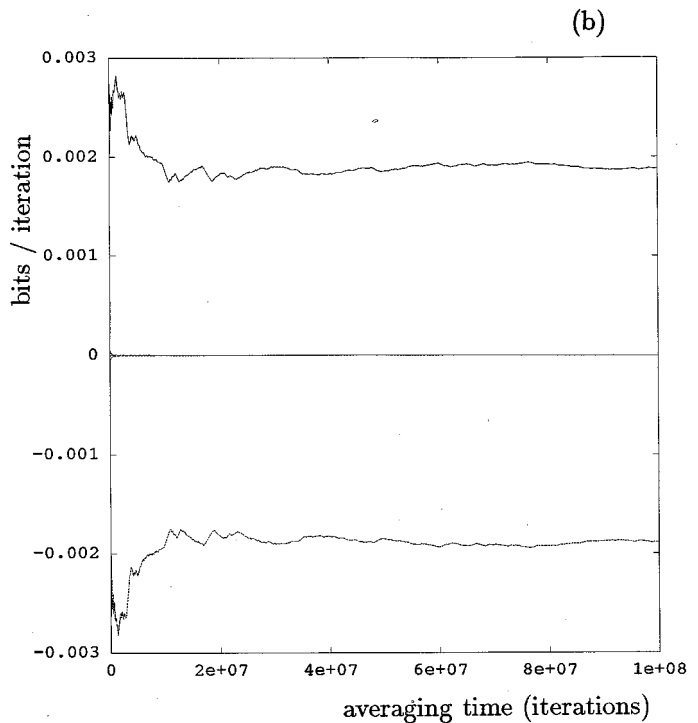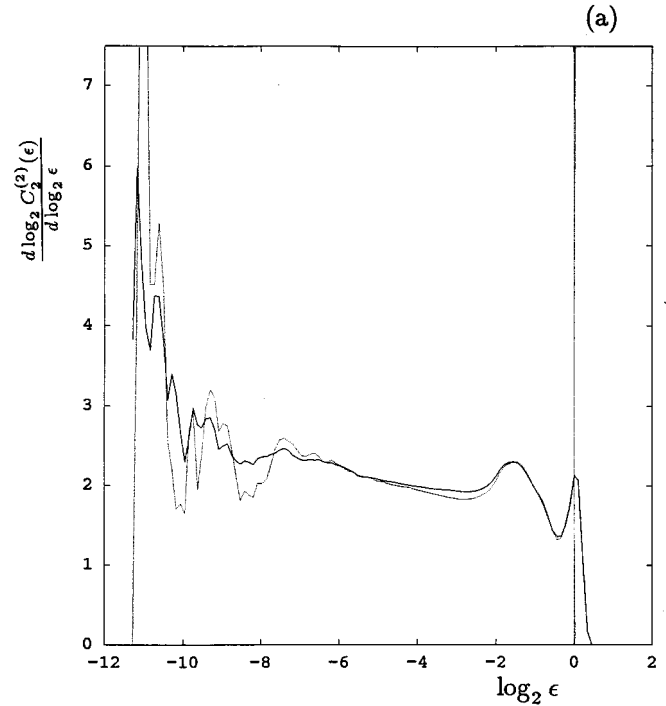
Fig. 8. The chain of eight small tori of Fig. 1b, when perturbed further by moving the initial conditions slightly outwards, yields an orbit which tends to "fill out" the region between them [see also Fig. 3(b)]; (a) the chaotic properties of this orbit are indicated by its correlation dimension (for 20 000 points (dotted) and 60 000 (solid)), which is seen to have a plateau near $D_2 \simeq 2.4$ at small radii; and (b) the largest Lyapunov exponent $\Lambda_{\max}$, which approaches the value 1.9×10^{-3} after $N = 10^8$ iterations (two exponents are almost zero).

when we searched that region using Laskar's frequency analysis [Laskar *et al.*, 1992; Laskar, 1993; Papaphilippou, 1996] we verified that, for several initial conditions yielding tube-tori, rotation numbers could not be identified, thus providing further evidence of small scale chaotic behavior in that region.

Finally, turning to chains of small rotational tori [obtained by perturbing long periodic orbits, lying on large rotational tori, see Fig. 1(b)], we have observed the following: Upon perturbing further their initial conditions or parameters, it often happens that the resulting orbit "wanders" about, "filling" the region between the small tori, in an apparently irregular fashion, see Fig. 3(b). That this motion is chaotic is demonstrated by its correlation dimension being $D_2 \simeq 2.4$ and its largest Lyapunov exponent converging to $\Lambda_{\max} = \max\{\Lambda_i\} \simeq 1.9 \times 10^{-3}$ after 10^8 iterations, as shown in Figs. 8(a) and 8(b), respectively. The details of our computations of D_2 and Λ_i's are given in the Appendix.

4. Conclusions

Ever since the discovery of the famous Greene's criterion for the study of the break-up of the golden mean torus in 2-D area-preserving twist maps [Greene, 1979] and MacKay's construction of the corresponding renormalization operator [MacKay, 1983], there have been several attempts to extend these results to higher-dimensional symplectic maps.

Some studies demonstrated, in special cases (like the "spiral mean" invariant torus), that, even though an approximate renormalization scheme can be constructed, no universal fixed point is found to exist [Kim & Ostlund, 1985; MacKay *et al.*, 1994]. Others showed that it is possible to study the breakdown of invariant tori of a 4-D "semi–standard" map by examining the convergence properties of Fourier series representations of these tori [Bollt & Meiss, 1993]. Finally, sequences of periodic orbits and their connection with resonance zones in phase space have been investigated in the case of reversible symplectic maps, satisfying the twist condition [Kook & Meiss, 1989].

In this paper, we have continued our study of the structure and breakdown of invariant tori of a 4-D symplectic mapping that arises in a realistic application [Vrahatis *et al.*, 1996] and does not fall in the class of twist maps. Our original goal was to examine the structure of tori by approximating them

with sequences of periodic orbits whose (rational) rotation numbers converge to the pair of irrational rotation numbers of an invariant torus.

Although we did obtain, using our periodic orbits, approximations of invariant tori about the origin, many of which had a similar morphology, we did not succeed in converging to the particular one we had set out to find, mainly because we could not locate periodic orbits with prescribed rotation numbers converging to the desired irrationals.

In the process, however, we did discover a number of interesting results, which constitute the main points of the present paper:

(1) Among the many *rotational tori* surrounding the origin which we constructed, some are located at large enough distances that small perturbations of them lead to orbits which eventually escape to infinity. Thus, given that orbits starting closer to the origin than the large ones are all seen to remain bounded (for at least 10^8 iterations), we can say that the large tori are useful, in the sense that they "outline" a region within which the motion is predominantly stable for all practical applications.

(2) We classified the invariant tori we found in different classes according to their morphology: Besides the rotational kind mentioned above, we also located *tube-tori* (in the form of twisted 2-D "tubes" in 4-D space) and *tori-chains* composed of small rotational tori. Cross-sections of these tori (in the slices of 4-D space) reveal a clear resemblance with island chains of 2-D area-preserving maps.

(3) We observed that, upon perturbation, large rotational tori can "break-up" into tube-tori or tori-chains, about which there is clear evidence of *small scale chaotic behavior*. Furthermore, tube-tori and tori-chains are formed around *invariant curves* consisting of either a single (1-D) loop, or a set of disjoint loops, respectively. Thus, one observes evident features of *self-similarity* under scaling, between large and small rotational tori, and single-loop and multi-loop orbits.

(4) We showed that it is possible to study these phenomena *quantitatively*, by calculating the correlation dimension, D_2, and the Lyapunov exponents, Λ_i, of the corresponding orbits: In the case of perturbations of large, rotational tori close to the escape region, we found that the values of $D_2 > 2$ and $\Lambda_{\max} > 0$ kept

increasing as the number of iterations increased, reflecting the diffusive character of the orbit. On the other hand, in the smaller scale regions of bounded, chaotic motion these quantities converged to definite values $D_2 > 2$ and $\Lambda_{\max} > 0$.

Clearly, a lot more remains to be done in the study of invariant tori of symplectic maps. For example, we found, in agreement with recent rigorous studies [Tompaidis, 1995], that the eigenvalues of our long periodic orbits clearly demonstrate that these orbits are very close to smooth invariant surfaces. Still, unless one is able to construct, for a general symplectic map, periodic orbits with prescribed rotation numbers, the validity of Greene's criterion in higher dimensions will remain an open question, and the precise conditions of torus breakdown will continue to elude us.

Acknowledgments

References

Badii, R. & Politi, A. [1984] "Intrinsic oscillations in measuring the fractal dimension," *Phys. Lett.* **A104**, 303–305.

Bernstein, L. [1971] *The Jacobi–Perron Algorithm. Its Theory and Application*, Lecture Notes in Mathematics **207**.

Bollt, E. M. & Meiss, J. D. [1993] "Breakup of invariant tori for the four dimensional semi-standard map," *Physica* **D66**, 282–297.

Bountis, T. C. & Tompaidis, S. [1991] "Strong and weak instabilities in a 4D mapping model of FODO cell dynamics," in *Future Problems in Nonlinear Particle Accelerators*, eds. Turchetti, G. & Scandale, W. (World Scientific, Singapore), pp. 112–127.

Contopoulos, G., Magnenat, P. & Martinet, L. [1982] "Invariant surfaces and orbital behaviour in dynamical systems of 3 degrees of freedom," *Physica* **D6**, 126–136.

Contopoulos, G. & Magnenat, P. [1985] "Simple three–dimensional periodic orbits in a galactic type potential," *Cel. Mech.* **37**, 387–414.

Corrigan, R., Huson, F. & Month, M. (eds.) [1982] See papers in *Physics of High Energy Accelerators* (A.I.P., New York), A.I.P. Conf. Proc. **87**.

Drossos, L., Ragos, O., Vrahatis, M. N. & Bountis, T. [1996] "Method for computing long periodic orbits of dynamical systems," *Phys. Rev.* **E53**, 1206–1211.

Eckmann, J.-P. & Ruelle, D. [1985] "Ergodic theory of chaos and strange attractors," *Rev. Mod. Phys.* **57**, 617–656.

Ellner, S. [1988] "Estimating attractor dimensions from limited data: A new method, with error estimates," *Phys. Lett.* **133**, 128–133.

Grassberger, P. & Procaccia, I. [1983a] "Characterization of strange attractors," *Phys. Rev. Lett.* **50**, 346–349.

Grassberger, P. & Procaccia, I. [1983b] "Measuring the strangeness of strange attractors," *Physica* **D9**, 189–208.

Greene, J. M. [1979] "A method for determining a stochastic transition," *J. Math. Phys.* **20**, 1183–1201.

Hénon, M. & Heiles, C. [1964] "The applicability of the third integral of the motion: Some numerical experiments," *Astron. J.* **69**, 73–79.

Isliker, H. [1992] "A scaling test for correlation dimensions," *Phys. Lett.* **A169**, 313–322.

Kim, S. & Ostlund, S. [1985] "Renormalization of mappings of the two-torus," *Phys. Rev. Lett.* **55**, 1165–1168.

Kook, H. & Meiss, J. D. [1989] "Periodic orbits of reversible symplectic mappings," *Physica* **D35**, 65–86.

Laskar, J., Froeschlé C. & Celletti, A. [1992] "The measure of chaos by the numerical analysis of fundamental frequencies. Application to the standard mapping," *Physica* **D56**, 253–269.

Laskar, J. [1993] "Frequency analysis for multidimensional systems. Global dynamics and diffusion," *Physica* **D67**, 257–281.

Lichtenberg, A. J. & Lieberman, M. A. [1983] *Regular and Stochastic Motion*, Applied Mathematical Sciences **38** (Springer-Verlag, New York).

MacKay, R. S. [1983] "A renormalisation approach to invariant circles in area-preserving maps," *Physica* **D7**, 283–300.

MacKay, R. S. & Meiss, J. D. (eds.) [1986] See papers in *Hamiltonian Dynamical Systems* (Adams Hilger, Bristol).

MacKay, R. S., Meiss, J. D. & Stark, J. [1994] "An approximate renormalization for the break-up of invariant tori with three frequencies," *Phys. Lett.* **A190**, 417–424.

Papaphilippou, Y. [1996] (private communication).

Schweiger, F. [1973] *The Metrical Theory of Jacobi–Perron Algorithm*, Lecture Notes in Mathematics **334**.

Smith, L. A. [1988] "Intrinsic limits on dimension calculations," *Phys. Lett.* **A133**, 283–288.

Takens, F. [1981] "Detecting strange attractors in turbulence," in *Dynamical Systems and Turbulence*,

Lecture Notes in Mathematics **898** (Springer, Berlin), pp. 366–381.

Takens, F. [1984] "On the numerical determination of the dimension of an attractor," in *Dynamical Systems and Turbulence*, Lecture Notes in Mathematics **1125**, (Springer, Berlin), pp. 99–106.

Theiler, J. [1986] "Spurious dimension from correlation algorithms applied to limited time-series data," *Phys. Rev.* **A34**, 2427–2432.

Theiler, J. [1991] "Some comments on the correlation dimension of $1/f^\alpha$ noise," *Phys. Lett.* **A155**, 480–493.

Todesco, E. [1994] "Analysis of resonant structures of four-dimensional symplectic mappings, using normal forms," *Phys. Rev.* **E50**, 4298–4301.

Tompaidis, S. [1995] "Approximation of invariant surfaces by periodic orbits in high-dimensional maps. Some rigorous results," preprint submitted for publication.

Turchetti, G. & Scandale, W. (eds.) [1991] See papers in *Future Problems in Nonlinear Particle Accelerators* (World Scientific, Singapore).

Vrahatis, M. N. [1988] "Solving systems of nonlinear equations using the nonzero value of the topological degree," *ACM Trans. Math. Software* **14**, 312–329.

Vrahatis, M. N. [1995] "An efficient method for locating and computing periodic orbits of nonlinear mappings," *J. Comput. Phys.* **119**, 105–119.

Vrahatis, M. N. & Bountis, T. C. [1994] "An efficient method for computing periodic orbits of conservative dynamical systems," in *Int. Conf. Hamiltonian Mechanics, Integrability and Chaotic Behavior*, ed. Seimenis, J. (Plenum Press, New York), pp. 261–274.

Vrahatis, M. N., Bountis, T. C. & Kollmann, M. [1996] "Periodic orbits and invariant surfaces of 4D nonlinear mappings," *Int. J. Bifurcation and Chaos* **6**(8), 1425–1437.

Vrahatis, M. N., Servizi, G., Turchetti, G. & Bountis, T. C. [1993] "A procedure to compute the periodic orbits and visualize the orbits of a 2D map," CERN SL/93–06 (AP).

Wolf, A., Swift, J. B., Swinney, H. L. & Vastano, J. A. [1985] "Determining Lyapunov exponents from a time series," *Physica* **B16**, 285–317.

Appendix

In this Appendix we describe the details of our computation of the correlation dimension and Lyapunov exponents described in Sec. 3. As is well known, the Correlation dimension D_2 is defined as the scaling exponent of the correlation integral $C_2^{(d)}(\epsilon)$,

$$C_2^{(d)}(\epsilon) \propto \epsilon^{D_2}, \quad \epsilon \to 0, \qquad \text{(A1)}$$

where the correlation integral is given by the double sum

$$C_2^{(d)}(\epsilon) = \lim_{M \to \infty} \frac{2}{(M-W)(M-W-1)}$$
$$\times \sum_{i=1}^{M-W-1} \sum_{j=i+W+1}^{M} \Theta(\epsilon - \|X^{(i)} - X^{(j)}\|), \qquad \text{(A2)}$$

according to Grassberger and Procaccia [1983a, 1983b]. The upperscript d denotes the dimension of state space, and it equals 4 in our case. The parameter W was introduced by Theiler [1986, 1991] in order to avoid biasing by temporally correlated points. This is achieved by setting W to a value larger than the auto-correlation time (defined as the lag of the first substantial change in the auto-correlation function, e.g. the first minimum). The arguments of Theiler are suited to the case where the temporal correlations decay reasonably fast (as for instance on a chaotic attractor). Here, however, we deal also with periodic orbits which are completely deterministic (predictable), and consequently all the points on a trajectory are correlated. Still, the parameter W is useful in our case, as it serves to avoid estimates which are dominated by the temporally close points, e.g. in the case of a curve-like orbit. In most of our calculations we used $W = 60$.

Usually, correlation dimensions are estimated from the time series of a single coordinate, from which the state-space dynamics is reconstructed (e.g. by the time-delay method of Takens [1981]). Here, however, since we have access to all the coordinates, we do not have to reconstruct the state space, and consequently no time-delay and no variation of the embedding dimension is needed, as it is known that $d = 4$, in (A1) and (A2).

The sets we investigate are described by a series of vectors with as many elements as the points of the orbit, M, cf. (16) (in the case of a period-p orbit, $M = p$). We then make use of the fact that the correlation integral shows the scaling behavior we are looking for already at intermediate scales, i.e. at finite radii, provided they are reasonably small compared to the size of the analyzed set. The scaling behavior of the correlation integral is best judged by inspecting plots of

$$D_2(\epsilon) = \frac{d \log_2 C_2^{(d)}(\epsilon)}{d \log_2 \epsilon}, \qquad \text{(A3)}$$

versus $\log_2 \epsilon$, so-called *slope plots*, where a dimension should reveal itself, in principle, as a straight, horizontal line, a so-called *plateau*, at small radii ϵ. Clearly, at large radii, effects due to the finite size of the set dominate the behavior, and at too small radii statistical fluctuations destroy any global features since one does not have enough data at small distances. Slope plots are notorious for showing considerable fluctuations in the meaningful range, yielding "plateaus" which are spoilt by oscillations and skew trends [Badii & Politi, 1984; Smith, 1988]. Thus, in order to extract an average dimension from the slope plots in an adequate way, we estimate correlation dimensions with the aid of the Maximum Likelihood (M-L) method [Takens, 1984; Ellner, 1988]. This alternative algorithm uses as input the range of radii where a power-law scaling behavior of the correlation integral is conjectured, for which it then yields an average dimension. The M-L estimate is superior to a fit of the slope-plot by a straight line, since the latter is just graphically motivated, while the M-L estimate is an intrinsic estimator.

Let us assume "convergence" of (A2) for a range of distances $\gamma_1 \leq \epsilon \leq \gamma_2$. Then the M-L formalism gives

$$D_2 = -\frac{m - K}{\displaystyle\sum_{ij=1}^{n} \ln(r_{ij}/\gamma_2)}, \qquad (A4)$$

where the number of distances $r_{ij} = \max[\|X^{(i)} - X^{(j)}\|; \gamma_1]$ is denoted by m, and K is the number of r_{ij}'s which are equal to γ_1. Distances $r_{ij} > \gamma_2$ are omitted. A prerequisite of the M-L formalism is that the distances are independent, which certainly would not be fulfilled if all the available distances ($m = (M - W)(M - W - 1)$) were taken into account. Ellner [1988] shows that if $m = M/2$ the estimate is best, since the distances then are most likely to be independent (M is the length of the original time series). The m distances we have used are chosen at random out of those fulfilling the constraint $|i - j| > W$, so that no temporally correlated vectors are taken into account (this allows us to avoid the possible biasing mentioned above).

Using the same probabilistic approach as for the M-L formalism, one can derive an intrinsic error formula for dimension estimates:

$$B = \frac{D_2 \, 1.96}{\sqrt{m}} \, \frac{\sqrt{1 + 2 \ln r_0^{D_2} \, r_0^{D_2} - r_0^{2D_2}}}{1 + \ln r_0^{D_2} \, r_0^{D_2} - r_0^{D_2}}, \qquad (A5)$$

with $r_0 = \gamma_1/\gamma_2$. The factor 1.96 stems from a 5% confidence interval used here [Ellner, 1988; Isliker, 1992]. The errors shown in Table 4 are calculated by this formula.

Turning finally to our computations of the Lyapunov exponents, we recall that they measure the degree of divergence of close trajectories in state space in the course of time. They are a direct tool to infer the presence of chaos: The latter is defined to be the case where at least one Lyapunov exponent is larger than zero.

The Lyapunov exponents can be estimated in our case by making use of the equations of the mapping. In the case of periodic orbits, they equal the logarithm of the eigenvalues of the return–Jacobian [see (14)], divided by the period of the orbit [Eckmann & Ruelle, 1985]. However, if the period is too high, the matrix product involved in calculating the return–Jacobian consists of many factors, and numerical errors rapidly accumulate especially in the calculation of the small eigenvalues.

An alternative way which has the additional advantage that it can be applied to nonperiodic orbits is provided by an algorithm proposed by Wolf *et al.* [1985], suitably modified for maps. In this application, the evolution of a *finite* 4-sphere of radius 1 is monitored in *tangent-space* following a trajectory in the region of interest. This sphere evolves under the action of the *linearized* equations into an ellipsoid, whose principal axes have lengths denoted by p_i. The ith Lyapunov exponent Λ_i is then determined by the formula [Wolf *et al.*, 1985]

$$\Lambda_i = \lim_{n \to \infty} \frac{1}{n} \log \frac{p_i(n)}{p_i(0)}, \quad i = 1, 2, 3, 4. \qquad (A6)$$

In the numerical implementation, this limit is replaced by an averaging procedure over many time-steps. Furthermore, the set of principal axes has to be reorthogonalized from time to time (for technical details of the procedure see [Wolf *et al.*, 1985]. We found it sufficient to evolve the sphere over a time 1 (the iteration time-step), to estimate the quotient in (A6), and to average these quotients over many time-steps, as convergence is rather slow (mainly due to the Lyapunov-exponents being small). This procedure yields numerically reliable estimates of the four Lyapunov exponents when the averaging is performed over about 50 000 time-steps, see Fig. 7 and Fig. 8(b).